Int J Adv Manuf Technol (2014) 73:409–419
DOI 10.1007/s00170-014-5833-4

ORIGINAL ARTICLE

# Predicting residual stresses and distortion during multisequence welding of large size structures using FEM

**R. Keivani · M. Jahazi · T. Pham · A. R. Khodabandeh · M. R. Afshar**

Received: 16 July 2013 / Accepted: 1 April 2014 / Published online: 22 April 2014


**Abstract** A three-dimensional thermomechanical finite element (FE) analysis is carried out to model and predict the influence of welding sequence on the generation of distortions and residual stresses in large size T-joints. To simulate industrial welding conditions, the influence of nine welding sequences on the magnitude of distortion in both the plate and the stiffener was investigated. The addition of new material during welding was simulated using an element "birth and death" technique, while the moving welding arc was considered as a volumetric heat source with a double ellipsoidal distribution. The investigated material is a structural steel used for fabrication of large size structures in the hydroelectric industry. To calibrate the model and validate the simulation results, welding-induced distortion for one sequence was initially modeled and the results were compared with experimental measurements. The optimum welding sequences for the base plate and the reinforcement plate were determined. The results indicated also that the predicted distortions obtained from three-dimensional FE analysis are in reasonable agreement with experimental measurements.

**Keywords** Welding simulation · Finite element modeling welding sequence · Welding deformation · Residual stress

R. Keivani · A. R. Khodabandeh · M. R. Afshar
Department of Material Engineering, Science and Research Branch, Islamic Azad University-Science and Research Branch, Tehran, Iran

M. Jahazi (✉) · T. Pham
Département de génie mécanique, École de Technologie supérieure, Montréal, Canada
e-mail: mohammad.jahazi@etsmtl.ca

## 1 Introduction

Metal inert gas welding (GMAW) is commonly used for the fabrication of large size engineering structures for hydro-mechanical applications. The movement of the heat source along the joint causes highly nonuniform temperature distributions across the joint and the parent metals. Therefore, the thermal expansion and contraction during heating and subsequent cooling as well as plastic deformation of the material at elevated temperatures result in inevitable distortions and residual stresses in the joint and the parent metals [1–3]. The problem becomes even more acute and critical when thick plates with a large number of welding passes are used [4]. Welding-induced distortion in T-joints manifests itself as in-plane deformation such as stretching and out-of-plane deformation in the form of bending, rotation, or buckling. The extent of deformations and residual stresses depends on the geometry and size of the joint, welding parameters, welding sequence, and applied structural boundary conditions [2].

The large number of variables and the complex interactions between them make difficult, if not impossible, the complete elimination of distortion and residual stresses upon welding in large size welded components. Process optimization generally is empirical and goes through many trial and error practices using various methods such as changes in weld process parameters, fixture modification, precambering, prebending, thermal tensioning, weld sequencing, control of weld consumable, and post-weld corrective methods [5]. However, many of these methods are costly and time consuming. In recent years, with the advent advanced numerical methods and powerful computational tools, it is possible to simulate the influences of various process parameters on the generation of post-weld distortion and residual stresses [6]. Specifically, finite element (FE) simulation

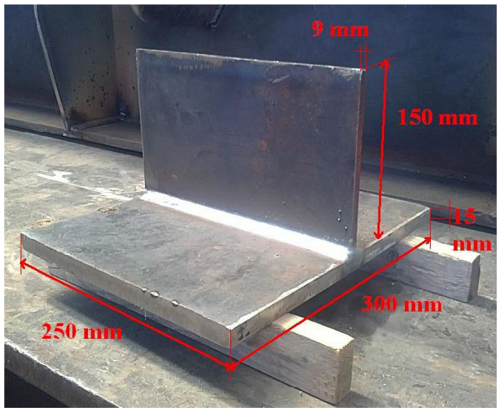


**Fig. 1** T-joint sample for experimental set-up

has become a widely used method for the prediction of welding distortions and residual stresses [2]. Comprehensive reviews on the stat-of-the-art in numerical modeling of welding have been reported in recent years by Lindgren [7] and Joy Varghese et al. [8]. Although a large number of numerical analyses have been conducted for predicting welding distortion on T-joints [3, 9, 10], however, little work has been reported on FE simulation of the influence of welding sequence on T-joints and most of the published literature on modeling has focused on plates or circumferential welds. For example, Anderson [11] studied the effect of welding sequence on the residual distortion of a panel in an 8-m long weld. Theoretical prediction of the effect of welding sequences on global deformation and end cracking has been reported by Deng and co-workers [12]. Recently, Gannon et al. [13] investigated the influence of welding sequence on residual stress development and distortion of flat-bar stiffeners used typically in ship hull construction and proposed a solution for a four welding sequence process.

In the present paper, the FE simulation software Abaqus is used to investigate the influence of up to nine welding sequence on the generation of residual stresses and distortions in a T-joint weld in a thick structural steel. The model is built on an elasto-plastic material with linear hardening behavior. Temperature distribution and heat transfer conditions are estimated based on existing validated models in the literature. The results obtained in the present analysis could be used as a basis for industrial applications because of the large number of welding sequences considered.

## 2 Experimental procedure

The configuration of the T-joint specimen used in the present investigation is shown in Fig. 1. The plate and stiffener are both made from a 0.16 % C (wt) structural steel with a composition equivalent to mild steel ST37-2 [14] as indicated in Table 1 .The dimensions of the plate were 300×250 mm with a thickness of 15 mm and those of the stiffener were 150×250 mm with a thickness of 9 mm. The stiffener was connected to the plate by 6-mm fillet welds deposited on both of its sides. GMAW was used to manufacture the T-joint with the welding process conditions reported in Table 2. Nine different welding sequences (“a” to “i”) were investigated as illustrated in Fig. 2. Sequence “a” was used as a reference for experimental validation of the FE modeling.

During the welding process, no external constraints were imposed on the assembly; as a result, the assembly was free to move in any direction. A cooling time of 120 s was left between each consecutive pass, and the welded specimen was left in the open air for cooling. Vertical deflections at the right and left spans of the welding line were measured using a digital caliper in directions “1” and “2” as shown in Fig. 3.

## 3 Material modeling assumptions

The material of the weld metal, the heat-affected zone, and the base metal are assumed identical. The thermal and mechanical properties of material were obtained from the literature and are illustrated as a function of temperature in Fig. 4 [14]. A thermal conductivity value of 300 W/m °C was assumed above the melt temperature to model for the stir effect due to the fluid flow in the molten pool [3, 15]. Solid-state phase transformation in steels is accompanied with crystallographic changes, which result in the generation of residual stresses and may even produce distortions [15]. The contribution of phase transformation to the generation of residual stresses in carbon steels could be significant and must be considered in any analysis. This is particularly true when the alloy possesses a

**Table 1** Chemical composition (wt%) of the investigated alloy

| C | Si | Mn | P | S | Cr | Ni | Mo | Cu | Co | Al |
|---|---|---|---|---|---|---|---|---|---|---|
| 0.16 | 0.2 | 0.46 | 0.012 | 0.01 | 0.06 | 0.11 | 0.02 | 0.2 | 0.01 | 0.01 |

**Table 2** Welding conditions

| Parameter | Current (A) | Voltage (V) | Welding speed (mm/s) |
|---|---|---|---|
| | 450 | 33 | 5 |

high yield strength (i.e., often high carbon or alloying elements levels) and near to room temperature phase transformation temperature [16]. However, in the present investigation, the alloy is low strength with low carbon and alloying elements. Moreover, its austenite-to-ferrite/pearlite transformation temperature is well above room temperature (around 500–600 °C). Hence, it can be reasonably concluded that, for the investigated alloy, the impact of solid-state phase transformation on residual stress generation, at least in a first approximation, could be considered negligible. Such approaches have also been used in recent years for successfully modeling the generation of residual stresses in welding of low alloy steels [17].

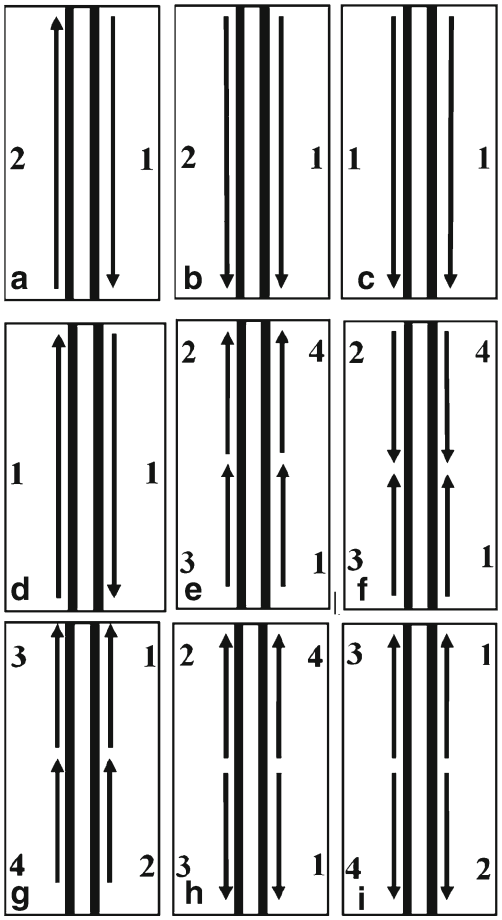


**Fig. 2** Investigated welding sequences

## 4 Three-dimensional FE modeling

A two-step solution procedure was adopted in the FE modeling approach. Initially, the temperature distribution and its history in the welding model were computed by the heat transfer analysis. Then, the temperature history was employed as a thermal load in the subsequent mechanical elastoplastic calculation of the residual stress field. In addition, an elastoplastic behavior with isotropic hardening law was assumed for the material. A relatively dense mesh is required through the thickness of the plate in the region surrounding the weld. In the region away from the location of the weld, the temperature gradient is significantly lower, and the mesh could be less dense, thereby reducing the calculation time. The complete model contains approximately 9,100 elements and 11,730 nodes as shown in Fig. 5. It must be noted that the same meshing configuration was used for all welding conditions.

## 5 Thermal analysis

Welding heat transfer analysis with given welding conditions was performed in the 3D model. In this step, temperature histories at each element nodes are computed during each time increment of the welding process. The governing equation for transient heat transfer during the welding operation is given by [18]:

$$\rho c \frac{\partial T}{\partial t}(x,y,z,t) = -\nabla . \overrightarrow{q}(x,y,z,t) + Q(x,y,z,t) \tag{1}$$

where $\rho$ is the density of the material (g/mm$^3$); $c$ is the specific heat capacity [J/(g °C)]; $T$ is the current temperature (°C); $q$ is the heat flux vector (W/mm$^2$); $Q$ is the internal heat generation rate (W/mm$^3$); $x$ , $y$, and $z$ are the coordinates in the reference system (mm); $t$ is the time (s); and $\nabla$ is the spatial gradient operator.

A volumetric heat source with a double ellipsoidal distribution was assumed for the application of the heat from the moving welding. The following equations and parameters were used for the analysis [19]:

For the front heat source:

$$Q(x',y',z',t) = \frac{6\sqrt{3} f_f Q_w}{\pi\sqrt{\pi} abc_f} \exp\left(-\frac{3x'^2}{a^2}\right) \exp\left(-\frac{3y'^2}{b^2}\right) \exp\left(-\frac{3z'^2}{c_f^2}\right) \tag{2}$$

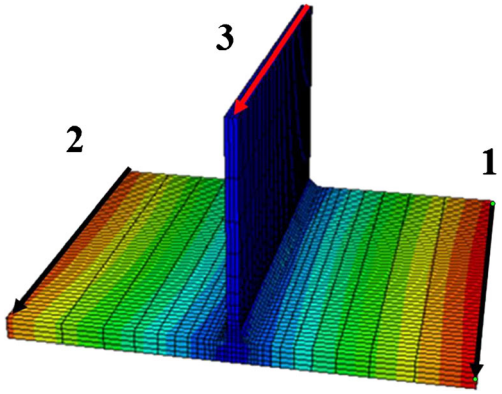


**Fig. 3** Locations for measuring

For the rear heat source:

$$Q(x',y',z',t)=\frac{6\sqrt{3}f_{\mathrm{r}}Q_{\mathrm{w}}}{\pi\sqrt{\pi}abc_{\mathrm{r}}}\exp\left(\frac{-3x'^{2}}{a^{2}}\right)\exp\left(\frac{-3y'^{2}}{b^{2}}\right)\exp\left(\frac{-3z'^{2}}{c_{\mathrm{r}}^{2}}\right). \tag{3}$$

where $x'$, $y'$, and $z'$ are the local coordinates of the double ellipsoid model aligned with the welded line; $f_{\mathrm{r}}$ and $f_{\mathrm{f}}$ are parameters that give the fraction of the heat deposited in the front and the rear parts, respectively. The two values are different because the temperature gradient in the front leading part is steeper than in the trailing edge. In the above equations, "a" represents the width of the heat source, "$b$" represents depth of the heat source, "$c_{\mathrm{f}}$" is the length of front ellipsoidal, and "$c_{\mathrm{r}}$" that of the rear ellipsoidal (Fig. 6). These parameters can be determined through experimental study of the weld pool and may be adjusted to create a desired melted zone according to the welding conditions [18]. In the present study, they were calculated for the welding sequence "a," and their values are reported in Table 3. The distance in front of the heat source (cf) was considered equal to one half the weld width and the distance behind the heat source (cr) equal to twice the width [19]. To validate the above assumptions, actual experimental measurements were made on a one sequence welding. Good agreement was observed between the measured values and the method proposed by Goldak et al., and hence, this approach was adopted for the present investigation.

$Q_{\mathrm{w}}$ is the power of the welding heat source and can be calculated from the following relation:

$$Q_{\mathrm{w}}=\eta IE \tag{4}$$

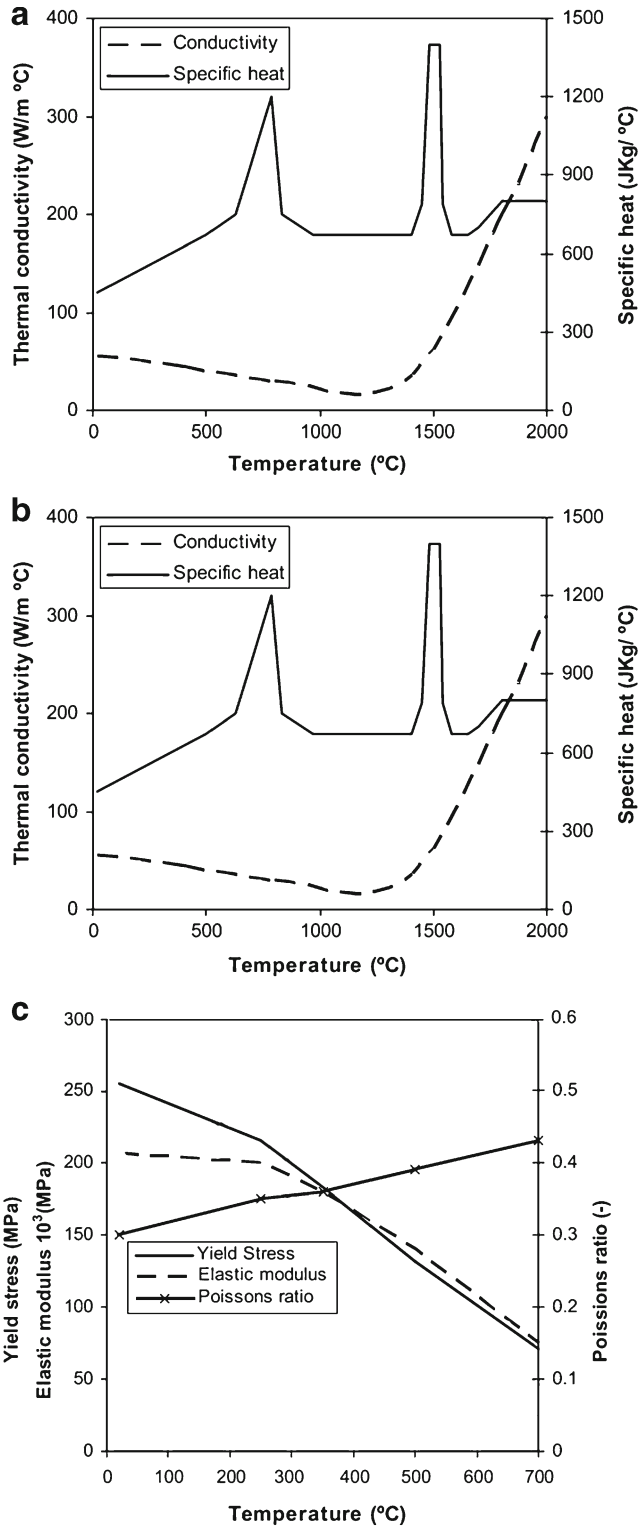


**Fig. 4** Material properties used for the welding simulations: **a** conductivity and specific heat, **b** yield stress and elastic modulus, and **c** thermal expansion coefficient [10]

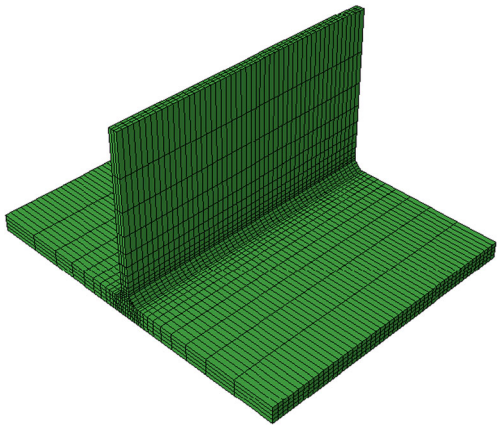

**Fig. 5** Mesh pattern used for the simulation

where $I$ is the welding current, $E$ the arc voltage, and $\eta$ the arc efficiency. The latter is assumed to be 80 % for the GMAW welding process.

The time-dependent element rebirth technique was employed to simulate the addition of the welding material during welding. The deactivation of elements was done by significantly reducing their contributions to the stiffness matrices and completely removing their contributions to the load vectors [10].

Newton's law was used to estimate heat losses ($q_c$) due to convection:

$$q_c = h(T - T_0). \tag{5}$$

and the Stefan–Boltzmann law was used for calculating the radiation heat losses ($q_r$):

$$q_r = \varepsilon\sigma\left(T^4 - T_0^4\right). \tag{6}$$

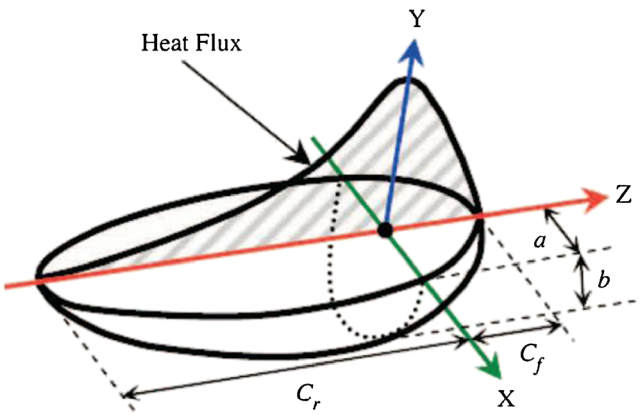


**Fig. 6** Double ellipsoid heat source configuration

**Table 3** Parameters of the heat source

| Parameter | Value (mm) |
|---|---|
| $a$ | 5 |
| $b$ | 7 |
| $c_f$ | 5 |
| $c_r$ | 20 |

In the above equations, $T_0$=25 °C is the ambient temperature; $\sigma$=5.67×10$^{-8}$ W m$^{-2}$ °C$^{-4}$ is defined as the Stefan–Boltzmann constant. The convection coefficient and the emissivity are defined to be $h$=15 W m$^{-2}$ and $\varepsilon$=0.7 [1].

## 6 Mechanical analysis

The solid model mesh used for the mechanical analysis was the same as the one used for the thermal analysis. The temperature history from the thermal analysis was used as a series of loads in the structural analysis, where each increment of weld deposition corresponded to one load step. Because phase transformation has an insignificant effect on the welding residual stress and distortion, the total strain (assuming negligible contribution from solid state phase transformation) can therefore be decomposed into three components as follows [18]:

$$\varepsilon^{total} = \varepsilon^e + \varepsilon^p + \varepsilon^{th}. \tag{7}$$

The components on the right-hand side of Eq. (7) correspond to elastic, plastic, and thermal strain, respectively.

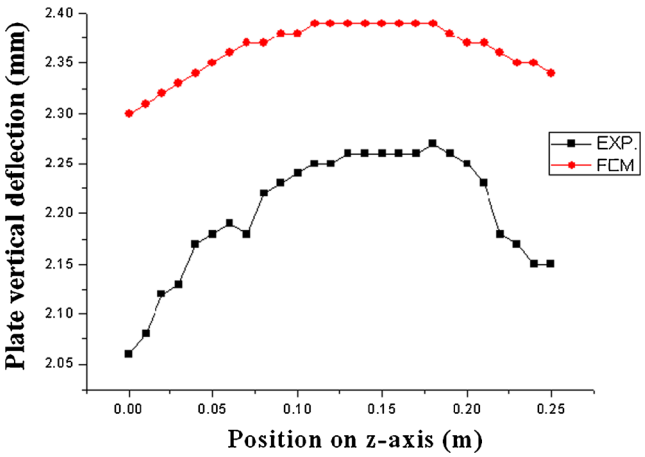


**Fig. 7** Plate vertical deflection distribution at the right span

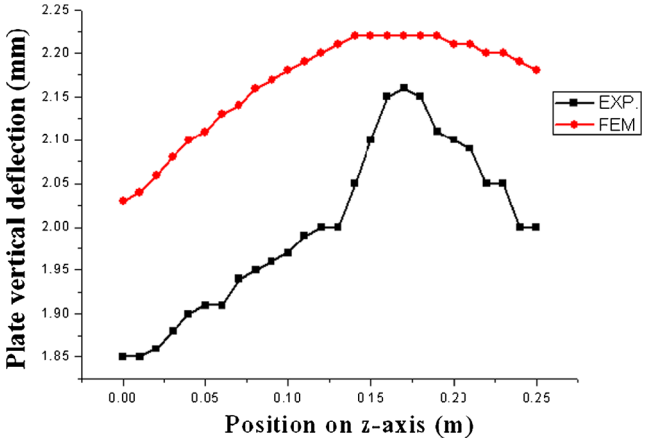


**Fig. 8** Plate vertical deflection distribution at the left span

Boundary conditions consistent with the experimental set-up were used in order to validate welding simulation results with experimental data. These consisted of assuming that the plate could deform freely in any direction with rigid body motions prevented in all directions.

## 7 Results and discussion

The finite element model for first welding sequence (sequence *a*) was validated by comparison of predicted deflections with experimental results. A comparison of vertical deflections of the plate at the right and the left spans (directions "1" and "2" shown in Fig. 3) is displayed in Figs. 7 and 8, respectively. The results indicate good agreement between computed and measured deflections with <10 % difference.

### 7.1 Effect of welding sequence on residual stress

Longitudinal residual stresses in the plate at mid-span are illustrated in Fig. 9 for the nine welding sequences. The results show that high tensile stresses in the vicinity of the yield stress

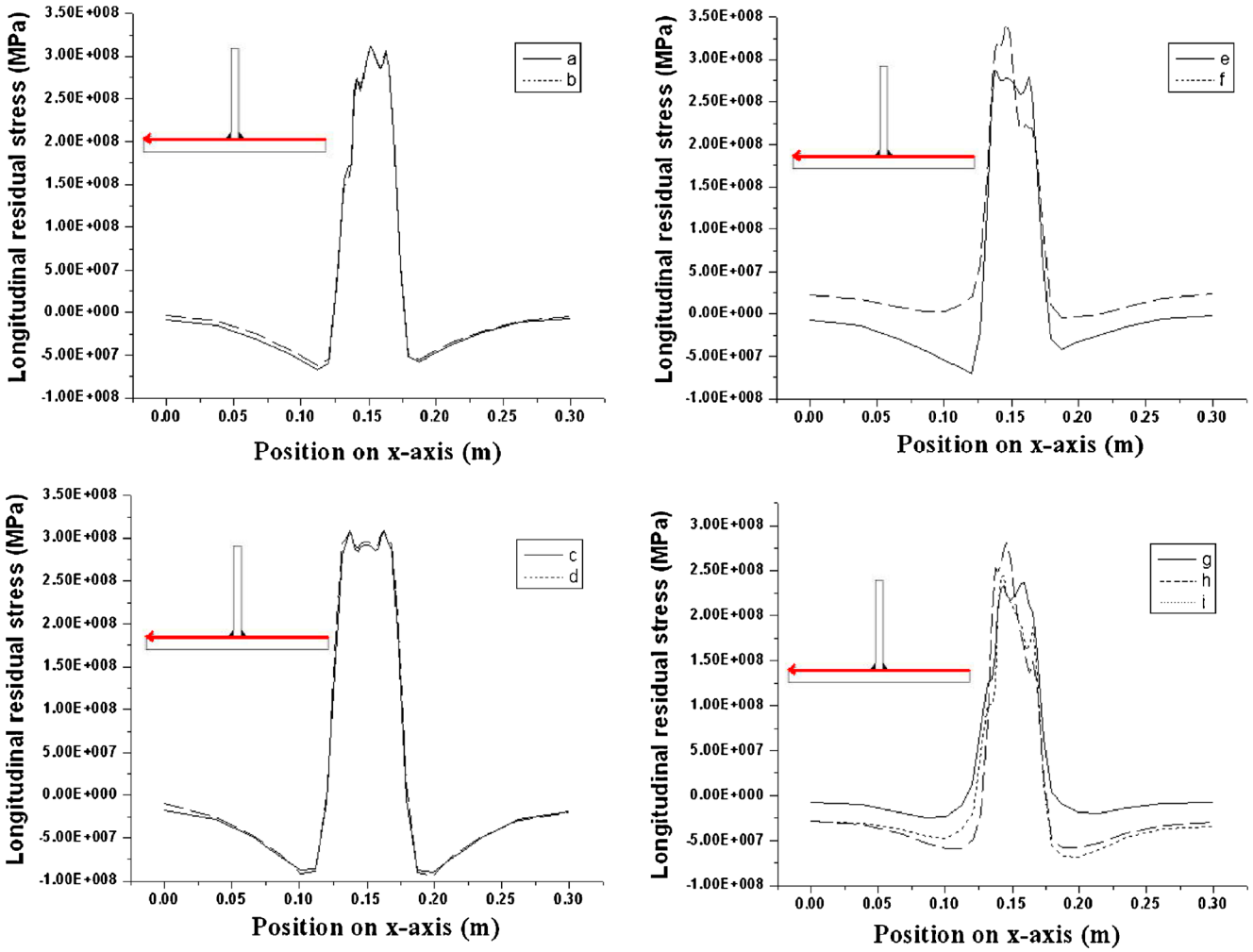


**Fig. 9** Longitudinal residual stresses in mid-span of the plate as a function of the welding sequence

of 265 MPa are present at the location of the weld. At this point, there is a rapid transition in the residual stress from tension to compression. The residual stress resulting from welding sequence "f" (343 MPa) is of greater magnitude than those resulting from other sequences. In Fig. 9 (1 and 2), the trend and the values for the residual stresses for welding sequences "a" and "b" and "c" and "d" are similar, respectively. It is worth noting that, in the above-mentioned cases, the welding directions are different for each case; however, because the residual stresses have been estimated at the center of the assembly, changes in the welding direction do not affect the estimation of the residual stresses. In addition, for the welding sequence "f," all welding directions are converging toward the same point; therefore, a different heat concentration will be produced, which will affect the intensity and distribution of the residual stresses when compared to other weld sequencing conditions.

Figure 9 (4) illustrates the distribution of residual stresses in the central region of the welded assembly for welding sequences "g," "h," and "i." It can be seen that, in this case, the intensity of the residual stresses are lower compared to the ones shown in Fig. 9 (1 and 2). An analysis of the welding conditions for these three conditions reveals that the heat concentration is minimum at the center as the welding directions move away from the center by compared to the sequence "f" where the heat was concentrated at the center. The above

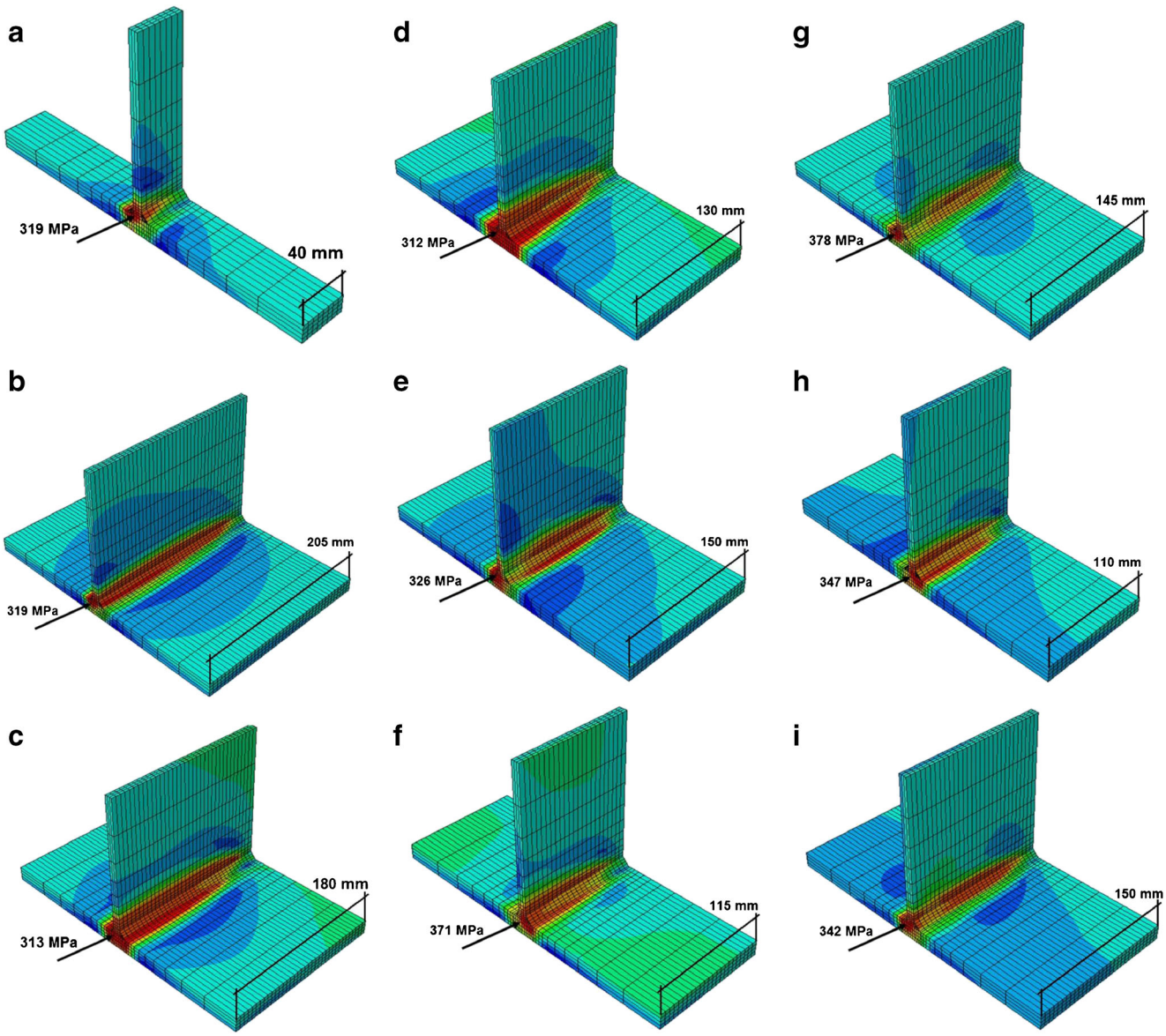


**Fig. 10** Residual stress levels for all welding sequences

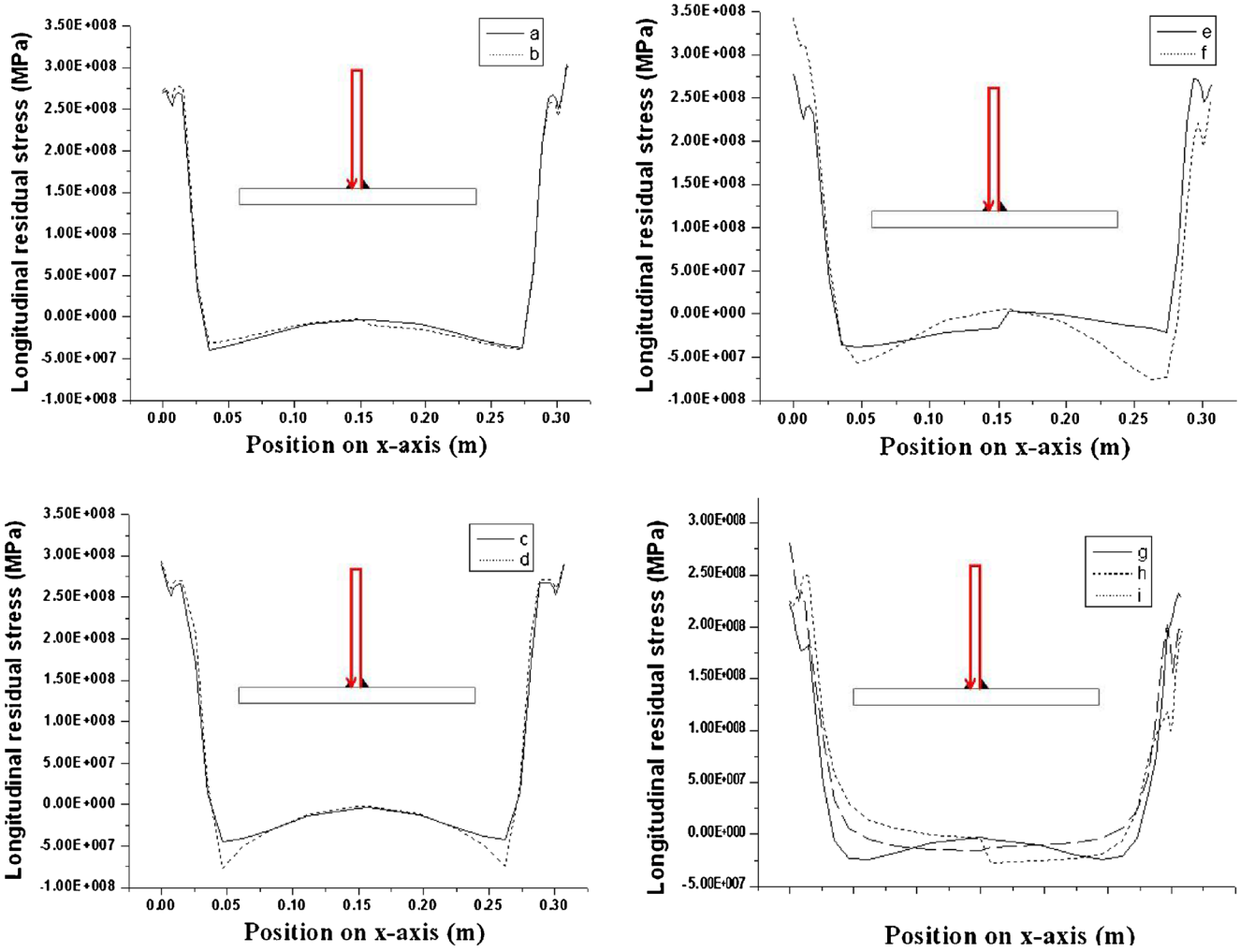


**Fig. 11** Longitudinal residual stresses in mid-span of the stiffener as a function of the welding sequence

results show in a quantitative manner the importance of welding sequence selection and order on the generation of residual stress. The maximum value for residual stress in the weld direction (S33) for weld sequences "a," "b," "c," "d,"

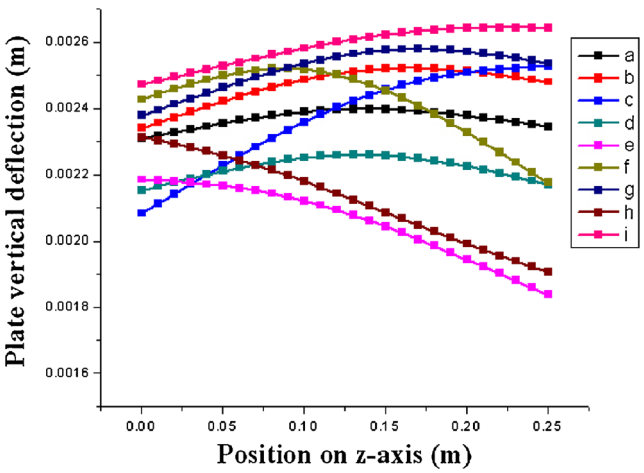


**Fig. 12** Vertical deflection of the plate (location 1 indicated in Fig. 3)

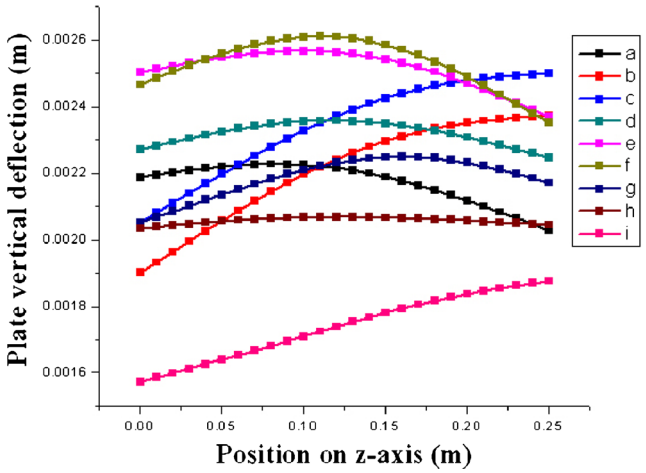


**Fig. 13** Vertical deflection of the plate (location 2 indicated in Fig. 3)

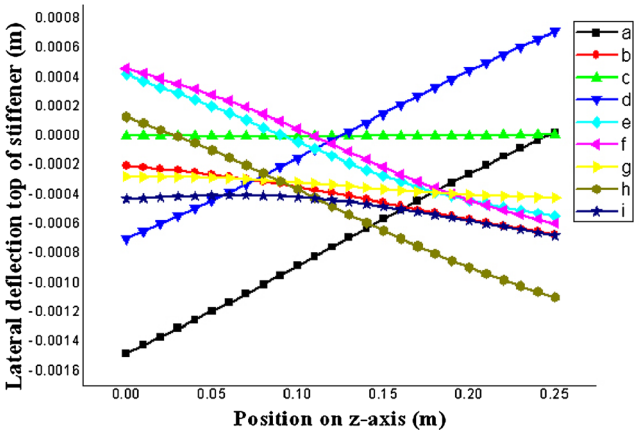


**Fig. 14** Lateral deflection of the stiffener (location 3 indicated in Fig. 3)

"e," "f," "g," "h," and "i" is 319, 319, 313, 312, 326, 371, 378, 347, and 342, respectively. As it can be seen, *f* and *g* sequences result in the highest residual stresses, which is probably due to the high thermal stresses generated because of the four welding passes used under these conditions. By contrast, the lowest levels of residual stresses are obtained with welding sequences "c" and "d" for which the two sides of the part were welded simultaneously resulting in lower thermal stresses by time unite. This is illustrated in Fig. 10, where the residual stress levels for all welding sequences are shown. The presented dimensions in Fig. 10 are measured from the free edge. For ease of comparison, only a section, with its distance from the start of the welding, is shown in this figure. It is interesting to note that, for welding sequences "a," "b," and "c," the geometrical location of the maximum residual stress is located at the side where the welding process ends (see also Fig. 2). This finding indicates that thermal stresses are the determining factor for the magnitude and distribution of residual stresses. The choice of welding sequences has been such that subsequent welding passes have played the role of a heat treatment for the previous one thereby affecting the thermal stresses and changing the residual stresses characteristics. This is further confirmed by considering the other welding sequences where the maximum residual stress level is attained in mid-section corresponding to the start and finish points of the welding process (i.e., points with very high levels of thermal stresses). Longitudinal residual stresses in the mid-span of the stiffener are illustrated in Fig. 11 for the nine welding sequences. The results are in agreement with those for the support plate and confirm that higher residual stresses are generated when weld sequence "f" is used.

### 7.2 Effect of welding sequence on distortion

Deflections of the plate in directions "1" and "2" (shown in Fig. 3) are illustrated in Figs. 12 and 13, and deflections of the stiffener in direction 3 (shown in Fig. 3) are illustrated in Fig. 14 for the nine welding sequences. Maximum vertical deflection, approximately 2.6 mm, was observed in direction 1 for welding sequence "i." By contrast, the minimum vertical deflection (approximately 1.83 mm) was found in direction 1 of welding sequence "e."

The results show that for sequences "b," "c," "d," "g," and "i" in direction 1, the deflection decreased from the start to end of the edge of the plate, while for sequences "e," "f," and "h," the opposite was found (i.e., the deflection increased from the start to the end of the edge). The maximum and minimum differences in deflections were 0.44 and 0.09 mm for sequences "c" and "a," respectively.

The maximum vertical deflection in direction 2 was found for the welding sequence "f" with a value of approximately 2.61 mm and the minimum for sequence "i" (1.57 mm). The evolution of deflection in direction 2 was not similar to that of 1. It was found that it has a decreasing trend from the start to the end for welding sequences "a," "d," "e," and "f," while it increased for sequences "i," "g," "b," "h," and "c." The analysis of the results indicate that if sequence "a" was selected as the base sequence, then the weld sequence "h" will lead to the minimum deflection in directions 1 and 2. It is interesting to note that, in sequences "e," "h," and "f" where a reduction in the amount of deflection was observed, the first and second passes were carried out in the opposite sides of the plate. This shows that deflection decrease in line with the welding heat flux. A similar analysis can be made for sequences "e" and "h" where passes 1 and 4 are carried out in the same side. The above results clearly demonstrate the importance of welding sequence selection.

The maximum deflection of stiffener in direction "3" with a value of approximately 1.48 mm resulted from the welding sequence "a" and the minimum deflection of approximately 0.71 mm in direction "2" resulted from welding sequence "d." The optimum conditions were obtained for the welding sequence "c" where both passes were carried out in one direction and at the same time resulting in more uniform temperature distribution in the material. By contrast, the worst deflections were obtained for sequences "a" and "d" in which the two welding passes were executed in opposite directions.

Figure 15 shows a post-weld overall view of deformed shapes including Von Mises stress contours for all nine welding sequences. It can be seen that the maximum stress is almost identical for all welding sequences. The variation of stress distribution as a function of the welding sequence, specifically for sequences "c" and "d," indicate that a more uniform stress distribution is observed along the weld line. This is due to the introduction of more uniform heat input into the material as a result of a judicious selection of the welding sequences.

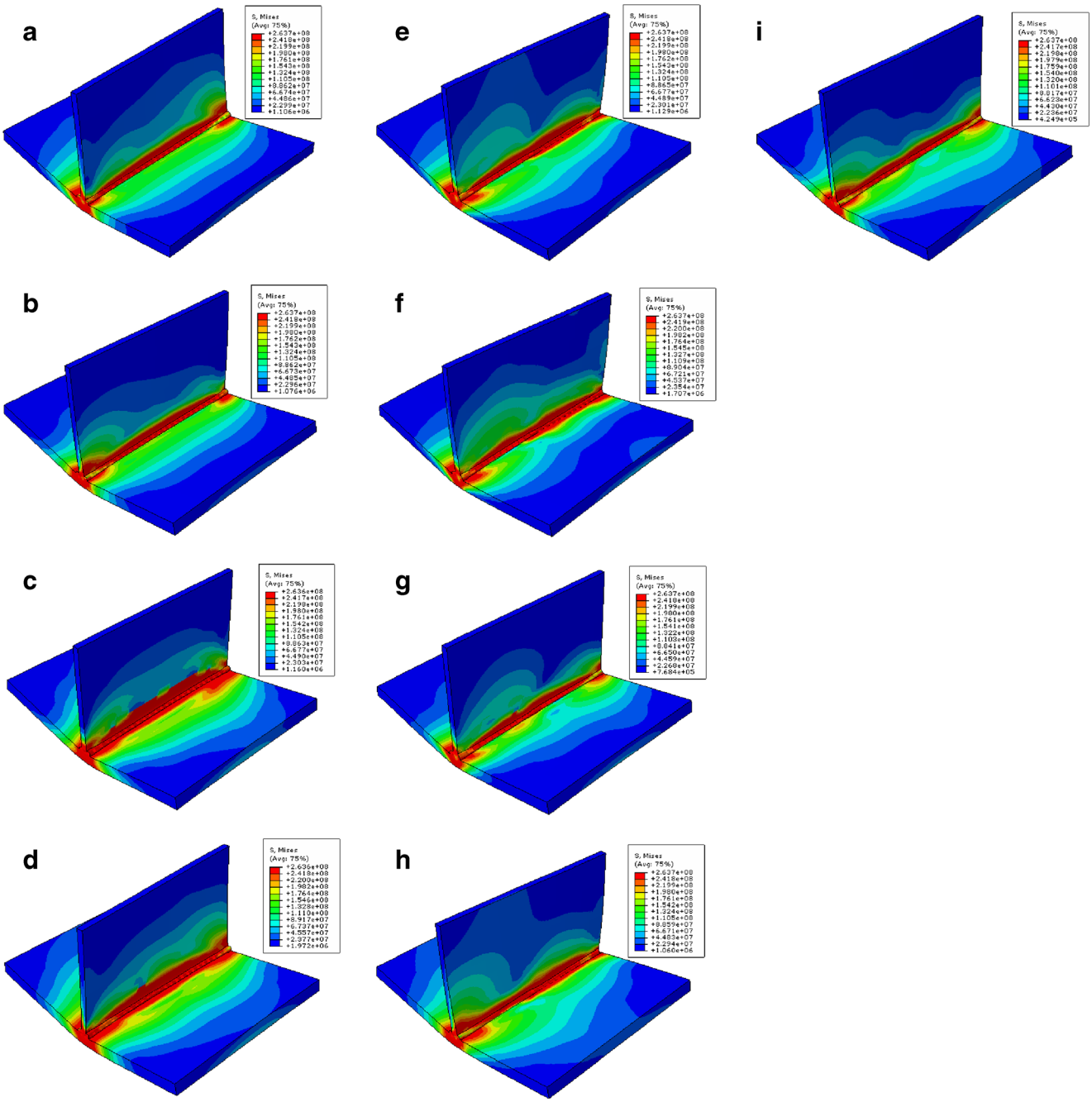


**Fig. 15** Deformed shapes with Von Mises stress contours for all welding sequences

## 8 Conclusions

The following conclusion can be drawn from the present investigation:

1. Predicted distortions from three-dimensional FE analysis are in reasonable agreement with experimental measurements.
2. If sequence "a" is selected for base sequence; then, sequence "h" leads to minimum deflection for both sides.
3. The optimum conditions were obtained when welding in one direction and at the same time (sequence "c").
4. Welding sequence influences the peak residual longitudinal stresses at mid-span.

## References

1. Gery D, Long H, Maropoulos P (2005) Effects of welding speed, energy input and heat source distribution on temperature variations in butt joint welding. Mater Process Technol 167:393–401
2. Sattari-Far I, Javadi Y (2008) Influence of welding sequence on welding distortions in pipes. Press Vessel Pip 85:265–274

3. Barsoum Z, Lundbak A (2009) Simplified FE welding simulation of fillet welds—3D effects on the formation residual stresses. Eng Fail Anal 16:2281–2289
4. Kou S (2002) Welding metallurgy. Department of Materials Science and Engineering University of Wisconsin
5. Masubuchi K (1980) Analysis of welded structures. Massachusetts Institute of Technology, USA
6. Feng Z (2005) Processes and mechanisms of welding residual stress and distortion, Woodhead publishing
7. Lindgren L-E (2006) Numerical modeling of welding. Comput Methods Appl Mech Eng 195:6710–6736
8. Joy Varghese VM, Suresh MR, Siva Kumar D (2013) Int J Adv Manuf Technol 64:749–754
9. Schenk T, Richardson IM, Kraska M, Ohnimus S (2009) A study on the influence of clamping on welding distortion. Comput Mater Sci 46:999–1005
10. Zaeem MA, Nami MR, Kadivar MH (2007) Prediction of welding buckling distortion in a thin wall aluminium T joint. Comput Mater Sci 38:588–594
11. Anderson LF (2000) Residual stresses and deformations in steels structures. Department of Naval Architecture and Offshore Engineering, Technical University of Denmark, Lyngby
12. Deng D, Serizawa H, Murakawa H (2001) Theoretical prediction of welding distortion considering positioning and the gap between parts. Trans JWRI 30(2):89–96
13. Gannon L, Liu Y, Pegg N, Smith M (2010) Effect of welding sequence on residual stress and distortion in flat-bar stiffened plates. Mar Struct 23:385–404
14. MatWeb. Online materials information resource. <http://www.matweb.com/>
15. Barsoum Z, Barsoum I (2009) Residual stress effects on fatigue life of welded structures using LEFM. Eng Fail Anal 16:449–467
16. Deng D (2009) FEM prediction of welding residual stress and distortion in carbon steel considering phase transformation effects. Mater Des 30:359–366
17. Hansen J L (2003) Numerical modeling of welding induced stresses. PhD thesis, Technical University of Denmark
18. Deng D, Murakawa H (2008) Prediction of welding distortion and residual stress in a thin plate butt-welded joint. Comput Mater Sci 43: 353–365
19. Goldak J, Chakravarti A, Bibby M (1984) A new finite element model for welding heat sources. Metall Mater Trans B 15:299–305